arXiv:hep-ex/9710013v1 16 Oct 1997

DIFFRACTION

E. GALLO
INFN Firenze, Largo Enrico Fermi 2
50125 Firenze, Italy
E-mail: gallo@desy.de

This report summarizes recent results on diffraction obtained at HERA, at the Tevatron and by the fixed target experiment E665. The measurements include vector meson production, inclusive diffraction at HERA and the pomeron structure function as inferred from the HERA and the Tevatron data.

1 Introduction

Diffractive interactions have recently attracted a lot of interest, following the results coming from HERA and the Fermilab experiments. Let me start with a brief introduction on what is diffraction.

Consider the total hadronic cross sections for the processes $pp, p\bar{p}, \pi^{\pm}p, K^{\pm}p, \gamma p$, as a function of the centre of mass (c.m.) energy $\sqrt{s}$ (see e.g. [1]). Their behaviour can be described as the sum of two components: $\sigma_{tot}^{h-h} = Ys^{-\eta} + Xs^{\epsilon}$, where the first term describes the decrease of the cross section with s at low energies, the second the slow increase at high energies. Donnachie and Landshoff [2] have performed a fit to all the available data at that time, obtaining a universal description of the hadronic cross sections with values $\eta \simeq 0.45$ and $\epsilon \simeq 0.08$. Recently Cudell et al.[3] have repeated the fit using only pp and $p\bar{p}$ data, obtaining the value $\epsilon = 0.096^{+0.012}_{-0.009}$, but claiming that any ϵ value in the range $0.07 - 0.11$ could describe the data. Finally the CDF experiment has measured ϵ with their own $p\bar{p}$ data at two different values of $\sqrt{s}$, obtaining a somewhat higher value, $\epsilon = 0.112 \pm 0.013$ [4].

This behaviour of the total hadronic cross section can be interpreted in terms of Regge theory [5]. The hadronic reaction $A + B \to C + D$ can be described by the exchange in the t-channel of a family of particles, such that the relevant quantum numbers are conserved. For these particles there is a linear relation between the spin J and the mass squared (t), which is of the form $J = \alpha(t) = \alpha(0) + \alpha' t$. The particles are lying on a so-called Regge 'trajectory', with intercept $\alpha(0)$ and slope α'. Regge theory predicts that the total cross section should behave as:

$$\sigma_{tot} \propto s^{\alpha(0)-1}. \tag{1}$$

The dependence of the elastic cross section with t, which is found to be exponential at small values of t, should behave as:

$$\frac{d\sigma_{el}}{dt} \propto (\frac{s}{s_0})^{2(\alpha(0)-1)} e^{bt}, \quad \text{with} \quad \mathrm{b} = \mathrm{b}_0 + 2\alpha' \ln(\mathrm{s}/\mathrm{s}_0) \tag{2}$$

The slowly decreasing term at low energy fitted by Donnachie-Landshoff corresponds to the intercept $\alpha_{I\!R} \simeq 0.5$ for reggeon exchange (i.e. the degenerate ρ, ω, f and a trajectories). The slow increase of the cross section at large energies corresponds to the so called pomeron

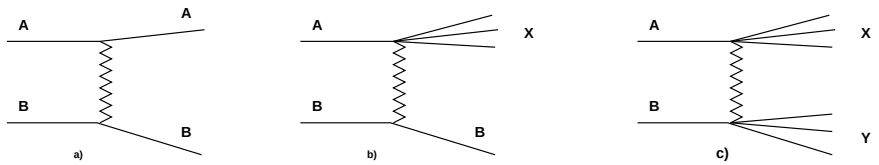

Figure 1: Feynman diagrams corresponding to pomeron exchange: (a) elastic, b) single dissociation, c) double dissociation.

trajectory, which has an intercept $\simeq 1.08$ according to the fit in [2], and which is the dominating term at high energies. The value of $\alpha'_{I\!P}$ was fitted to be $\simeq 0.25$ GeV^{-2}, implying that the exponential t distribution becomes steeper as the energy increases (an effect called 'shrinkage'). There are no known particles corresponding to the pomeron, except a glueball candidate from the WA91 experiment [6] which would lie on its trajectory.

The $d\sigma/dt$ distribution in proton-proton elastic scattering has a characteristic behaviour, with an exponential fall-off, a dip and a second exponential, which is very similar to the pattern of diffraction of light by a circular aperture (see e.g. [7]). Therefore the name of *Diffraction* was used to indicate pomeron exchange.

The processes mediated by pomeron exchange can be classified as elastic, single dissociation and double dissociation as shown is fig. 1. In this report I will concentrate on elastic vector meson production and the single dissociation process. In the latter process, the particle 'B' is either a proton or anti-proton, which remains intact after the interaction, carrying almost all of the initial beam momentum; the particle A can be either a proton or antiproton at the Tevatron, or a photon or virtual photon at HERA and E665. In Vector Meson Dominance (VDM) models or in perturbative QCD (pQCD), the photon can fluctuate into hadrons, so that the $\gamma^{(*)}p$ interaction can be seen as a hadron-hadron interaction. From the processes pictured in fig. 1 it is also clear that the pomeron has to carry the quantum numbers of the vacuum: in particular it is a colour-singlet and one expects to see a rapidity gap (i.e. a region with no particles) between the leading particle B and the dissociative system X. The experiments at HERA and the Tevatron have large rapidity coverage and have or are planning to have a forward proton spectrometer to measure the scattered leading proton.

There are still many open questions in diffraction on the nature of the pomeron. One of the main issues is whether the pomeron is 'soft', by which it is generally meant that its intercept is close to 1.08, or whether is it 'hard', which corresponds to an effective intercept greater than 1.08. In pQCD models [8], the dependence of the cross section with the energy is driven by the rise of the gluon density at low x, where x is the Bjorken variable, and a steep increase with the energy may be expected. This will be discussed in the first sections. Another issue is whether the pomeron can be treated as a 'particle' with a partonic structure, as first suggested in [9], and, in such case, what is the pomeron structure function. This question will be addressed in the second part of this report, together with a test of factorization.

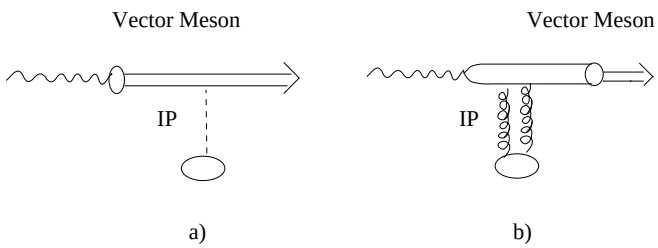

Figure 2: Elastic vector meson production in deep inelastic scattering as seen in soft pomeron+VDM models (a) or in perturbative QCD models (b).

2 Elastic Vector Meson Production

Elastic vector meson production in $e(\mu)p$ collisions, $e(\mu)p \to e(\mu)Vp$, is the ideal reaction to study the interplay between the soft and the hard regime. The electron or the muon emits a photon which fluctuates into a vector meson and interacts with the proton via pomeron exchange.

In the soft non perturbative regime [10], the process is seen as the fluctuation of the photon into a vector meson, which interacts with the proton via the exchange of a soft pomeron (see fig. 2a). The dependence of the cross section with the γp c.m. energy W is, assuming a pomeron intercept of 1.08 and $\alpha' \simeq 0.25$ GeV^{-2},

$$\sigma(\gamma p \to Vp) \propto \frac{(W^2)^{2(\alpha_{I\!P}(0)-1)}}{b_0 + 2\alpha' \ln(W^2/W_0^2)} \simeq W^{0.22}. \tag{3}$$

However, whenever a hard scale is involved in the process, which could either be the virtuality of the photon Q^2, the mass of the quark in the vector meson or the square of the four momentum transfer at the proton vertex t, the process can be calculated in perturbative QCD (see e.g. [11]). In this framework the pomeron is seen, at leading order, as a two-gluon system in a colour-singlet state, which interacts with the $q\bar{q}$ system of the vector meson (see fig. 2b). The total cross section, or the longitudinal part of the cross section in the case of virtual photons ($Q^2 > 0$), is proportional to the square of the gluon density in the proton at low x:

$$\sigma_{(L)}(\gamma^{(*)}p \to Vp) \propto [xG(x, Q^2)]^2 \simeq W^{4\lambda} \simeq W^{0.8}, \tag{4}$$

where $xG(x) \simeq x^{-\lambda} \simeq x^{-0.2}$ and $W^2 \simeq Q^2/x$ at low x. HERA has the possibility to study this process by varying the different scales Q^2, M_V and t (the latter is not discussed here).

Figure 3 shows a compilation of cross sections for different vector mesons in photoproduction ($Q^2 \simeq 0$) as a function of the γp c.m. energy W. The HERA data from the H1 and ZEUS experiments extend the region in W by almost an order of magnitude compared to fixed target experiments. A dependence of the form $W^{0.22}$ can describe the behaviour of the $\sigma(\gamma p \to Vp)$ cross section with the energy for the lightest vector mesons (ρ^0, ω and

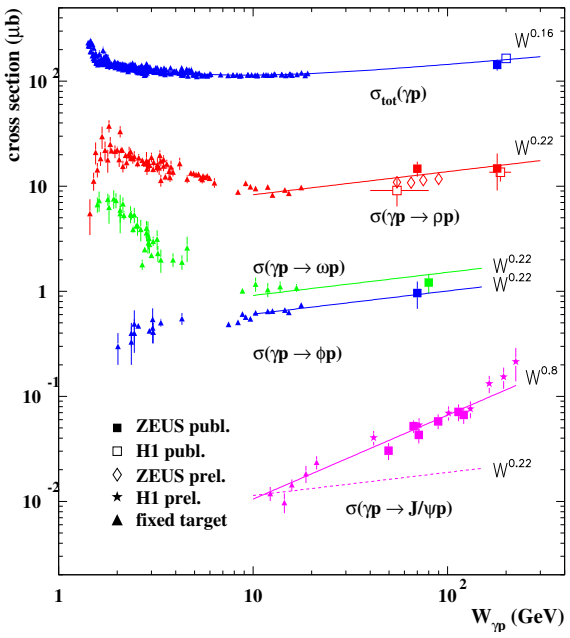

Figure 3: Cross sections for elastic vector meson production in photoproduction as a function of W.

ϕ). However the J/ψ photoproduction cross section shows definitely a steeper dependence, evident also within the HERA data (for instance the line $W^{0.8}$ would describe the data).

Figure 4 shows a compilation of recent results on ρ^0 production cross sections as a function of the $\gamma^* p$ c.m. energy W. For low values of Q^2 ($Q^2 \lesssim 2$ GeV^2) there is a nice continuation between the recent data published by the E665 Collaboration [12] (fixed target μp scattering) at low W and the preliminary HERA data at higher values of W: the soft pomeron approach describes the dependence of the cross section as a function of energy. At higher values of Q^2 ($Q^2 \gtrsim 5$ GeV^2) the situation is less clear. There is some discrepancy between the E665 and the older NMC data at $Q^2 \simeq 6$ GeV^2 [13], which give different conclusions when these data are extrapolated to the HERA energies and compared to the H1 and ZEUS data. One can however look at the HERA data alone: the ZEUS Collaboration has fitted the preliminary 95 data with the form W^a for four different Q^2 values, obtaining a value of a which increases gradually from $a \simeq 0.18$ at $Q^2 = 6$ GeV^2 to $a \simeq 0.77$ at $Q^2 \simeq 20$ GeV^2, however with large errors.

In summary the mass of the charm in the J/ψ photoproduction may give the hard scale, causing the steep rise of the cross section with W, while for the production of the light vector meson ρ^0 there is an indication that increasing Q^2 perturbative QCD starts to play a role, even if there are still experimental uncertainties. In principle this process is a very important reaction to determine the gluon density at low x, as the cross section has a quadratic dependence on $xG(x, Q^2)$, but there are still theoretical uncertainties in this determination. It will be interesting to study further this process with more statistics

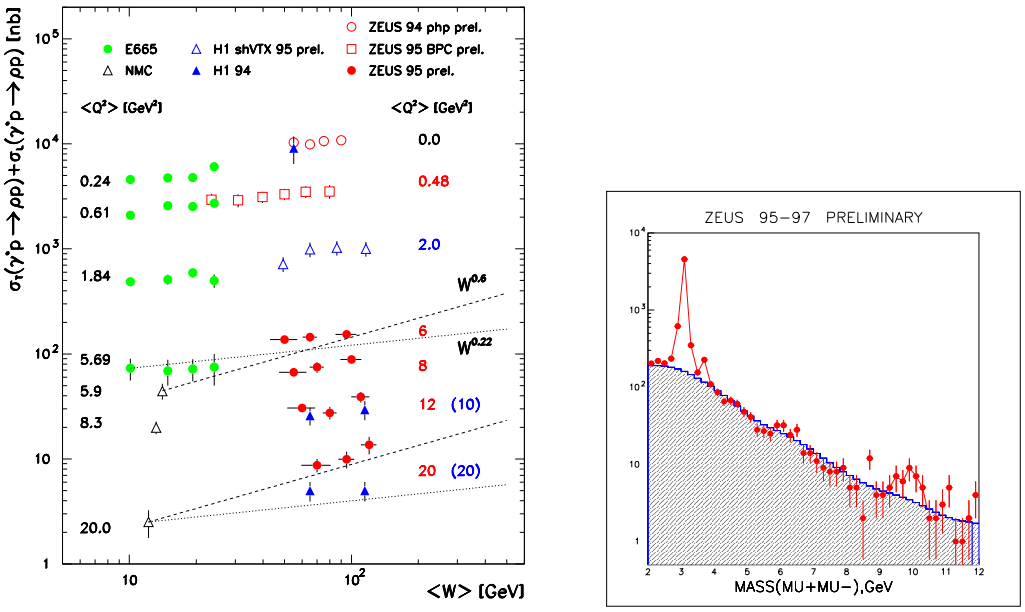

Figure 4: On the left: cross section for ρ^0 production as a function of W for different Q^2 values. On the right: invariant mass of $\mu^+\mu^-$ events observed in the photoproduction 95-97 ZEUS data, in the range $2-12$ GeV. The peaks due to the J/ψ, the ψ' and the Υ resonances are visible.

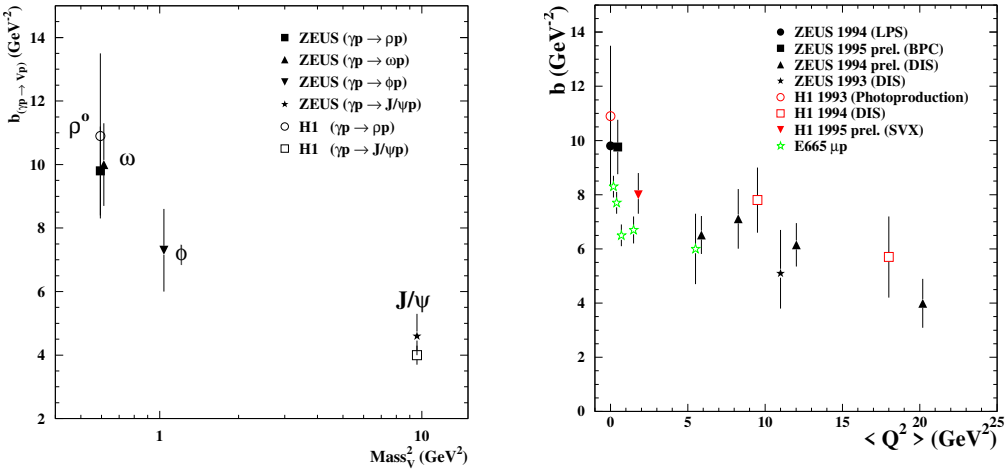

Figure 5: Dependence of the slope parameter b as a function of the mass squared of the vector meson in photoproduction (left) and as a function of Q^2 for the ρ^0 (right).

and with other vector mesons. The ZEUS Collaboration has observed in the 1995-1997 photoproduction data of the order of 20 Υ events in the $\mu^+\mu^-$ channel (fig. 4). The cross section, assuming that most events originate from the $\Upsilon(1S)$ state, is:

$$\sigma(\gamma p \to \Upsilon N, M_N \lesssim 4\ GeV) = 0.9 \pm 0.3 \pm 0.3\ nb, \tag{5}$$

in the kinematic range $80 < W < 280$ GeV and $Q^2 < 4$ GeV^2, where N indicates the proton or the low mass state in which the proton dissociates. For $M_N \lesssim 4$ GeV^2 this proton dissociation background contributes for $\lesssim$30% to the elastic Υ production. The cross section is of the order of 1% of the J/ψ photoproduction cross section, as predicted in some perturbative QCD models [14].

Another interesting variable to investigate the role played by perturbative QCD is the slope parameter b in the exponential t dependence of the cross section ($d\sigma/dt \propto e^{-b|t|}$ at low $|t|$). This is shown in fig. 5 as a function of the mass of the vector meson in photoproduction and as a function of Q^2 for the ρ^0. The slope parameter b, which is related to the transverse size of the interaction ($b \propto R_p^2 + R_V^2$, where the radius of the proton R_p^2 corresponds to $\simeq 4$ GeV^{-2}), is seen to decrease with the mass or with Q^2. This corresponds to the pQCD picture in which, at low x, the photon fluctuates into the $q\bar{q}$ system well before the target; the proton then interacts via the two-gluon exchange with the $q\bar{q}$ system, whose transverse size decreases with increasing Q^2 or the mass of the vector meson. The process then becomes a short distance process and therefore calculable in pQCD.

3 Single Photon Dissociation at HERA

The single photon dissociation process at HERA, $ep \to eXp$, is an important tool to study the nature of the pomeron and its possible partonic structure. The diagram of the process is drawn in fig. 6: the electron emits a quasi-real photon ($Q^2 \simeq 0$) or a virtual photon (for $Q^2 > 0$) which interacts with the proton via exchange of a pomeron and dissociates into a system X. The square of the four-momentum transfer t at the proton vertex is typically small ($|t| \lesssim 1$ GeV^2) and the scattered proton carries almost all the initial beam momentum. As the pomeron is a colour-singlet state, a rapidity gap in particle flow is expected between the scattered proton direction and the system X. These signatures are used to select inclusive diffractive events.

H1 selects diffractive events by requiring a large rapidity gap between the system X and the system N going into the forward proton direction, where N can either be the scattered proton or the state into which the proton dissociates. The forward pseudo-rapidity coverage of H1 is $3.4 < \eta < 7.5$ [a], constraining the mass of the system N to be less than 1.6 GeV. The cross section that H1 quotes contains thus a 5% contamination due to double dissociation. ZEUS uses instead two different methods for the selection of single $\gamma^{(*)}$ dissociation events. The first method exploits the different behaviour of the M_X distribution for non diffractive and diffractive events. The $\ln M_X^2$ distribution can be written as the sum of two components: at high M_X, the $\ln M_X^2$ distribution exhibits an exponential fall-off for normal DIS events;

[a] The pseudo-rapidity η is defined as $-\ln(\tan(\theta/2))$, where θ is the polar angle measured with respect to the proton direction.

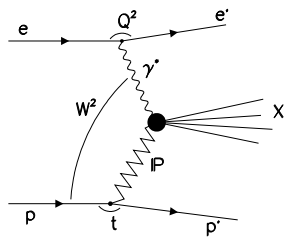

Figure 6: Feynman diagram for single dissociation at HERA.

at low M_X it is approximately flat as expected for diffractive events. The second method is based instead on the measurement of the scattered proton in the leading proton spectrometer (LPS), requiring a proton with a fraction of the incoming beam energy x_L close to 1. This latter method has the advantage to allow a measurement of t, but the acceptance is small.

3.1 Photoproduction

Following Regge phenomenology[15], the double differential cross section for the process $\gamma p \to Xp$ can be written as:

$$\frac{d\sigma}{dtdM_X^2} = (\frac{1}{M_X^2})^{\alpha_{I\!P}(0)}(W^2)^{2\alpha_{I\!P}(0)-2}e^{-b|t|} \tag{6}$$

$$b = b_0 + 2 \cdot \alpha' \ln(W^2/M_X^2). \tag{7}$$

The dependence of the diffractive γp cross section on t has been measured by ZEUS in the kinematic range $176 < W < 225$ GeV, $4 < M_X < 32$ GeV, $0.07 < |t| < 0.4$ GeV^2 and $0.97 < x_L < 1.02$. The cross section exhibits an exponential shape, and a fit with the form $e^{-b|t|}$ yields the value for the slope parameter $b = 7.3 \pm 0.9 \pm 1.0$ GeV^{-2} (preliminary). The value can be compared to earlier results obtained in γp interactions by the E612 Collaboration [16], at lower values of W ($< W >= 14$ GeV) and in a different t range ($0.02 < |t| < 0.1$ GeV^2). The formula (7) with $\alpha' = 0.25$ GeV^{-2} describes the dependence of b on the ratio W^2/M_X^2; however the experimental errors are still large.

The dependence of the differential cross section on M_X^2 gives instead a measurement of the pomeron intercept at $Q^2 \simeq 0$. The measurement has been performed both by H1 and ZEUS at $W \simeq 200$ GeV, obtaining $\alpha_{I\!P}(0) = 1.07 \pm 0.02(stat.) \pm 0.02(syst.) \pm 0.04(model)$ (H1)[17] and $\alpha_{I\!P}(0) = 1.12 \pm 0.04(stat) \pm 0.08(syst)$ in the range $8 < M_X < 24$ GeV (ZEUS)[18]. Both values are compatible with the soft pomeron intercept.

3.2 Deep Inelastic Scattering

As already mentioned, the measurement of inclusive single diffractive dissociation in DIS can give information on the nature of the pomeron and, assuming that it can be treated

as a particle, the virtual photon can probe its partonic structure. The kinematics of the process (see fig. 6) is described, in addition to the usual DIS variables Q^2, x and $y = Q^2/xs$, by the two variables:

$$x_{I\!P} \simeq \frac{M_X^2 + Q^2}{W^2 + Q^2} \simeq 1 - x_L \ , \quad \beta \simeq \frac{Q^2}{Q^2 + M_X^2} \tag{8}$$

as well as by t. For pure pomeron exchange, $x_{I\!P}$ is the fraction of the proton momentum carried by the pomeron and β can be interpreted as the fraction of pomeron momentum carried by the struck quark (the analogue of x Bjorken for the proton). The cross section for this process can be written, in analogy to normal DIS events, in terms of a diffractive structure function $F_2^{D(4)}$:

$$\frac{d^4\sigma^D_{(ep\to e'Xp')}}{d\beta dQ^2 dx_{I\!P} dt} = \frac{4\pi\alpha^2}{\beta Q^2}(1 - y + \frac{y}{2})F_2^{D(4)}(\beta, Q^2, x_{I\!P}, t) + \delta_L + \delta_Z, \tag{9}$$

where δ_L and δ_Z are the contributions due to the longitudinal structure function and to the Z exchange, respectively. These will be neglected in the kinematic range of the measurements described here. In factorizable models where the pomeron is treated like a particle (see e.g. [9]), the diffractive structure function can be written as the product of two terms:

$$F_2^{D(4)} = f^{I\!P}(x_{I\!P}, t)F_2^{I\!P}(\beta, Q^2), \tag{10}$$

where the the flux $f^{I\!P}$ depends only on $x_{I\!P}$ and t and $F_2^{I\!P}$, which can be interpreted as a pomeron structure function, depends only on β and Q^2. In most of the measurements the scattered proton is usually not detected and t cannot be measured, therefore the structure function $F_2^{D(3)}$ is defined, obtained by integrating $F_2^{D(4)}$ over t. Equation (10) becomes then

$$F_2^{D(3)} \propto \frac{1}{{x_{I\!P}}^a} F_2^{I\!P}(\beta, Q^2), \tag{11}$$

where the $x_{I\!P}$ exponent can be related to the pomeron intercept $\overline{\alpha_{I\!P}}$, integrated over the t range, with the relation $a = 2\overline{\alpha_{I\!P}} - 1$. If factorization holds, a is independent of β and Q^2.

ZEUS has measured the structure function $F_2^{D(4)}$, using the 1994 data in which the scattered proton was measured in the LPS, in the kinematic range $x_L > 0.97$,$5 < Q^2 < 20$ GeV^2,$0.015 < \beta < 0.5$ and $0.073 < |t| < 0.4$ GeV^2. The result is shown in fig. 7 where the function $x_{I\!P}F_2^{D(4)}$ is plotted as a function of $x_{I\!P}$ in four β bins. Figure 8 shows the structure function $F_2^{D(3)}$ plotted as $x_{I\!P}F_2^{D(3)}$ as a function of $x_{I\!P}$, obtained by integrating $F_2^{D(4)}$ over t. Together with the LPS data, the points obtained with the M_X method are also shown. The LPS data extend the measurements to higher values of $x_{I\!P}$ and lower values of β, as higher values of M_X can be reached with this method. The two measurements agree in the region of overlap both in shape and in normalization. The $x_{I\!P}$ dependence seems to change with the $x_{I\!P}$ range, having a negative slope for the function $x_{I\!P}F_2^{D(3)}$ at low $x_{I\!P}$ values, and becoming flat or even positive at higher $x_{I\!P}$.

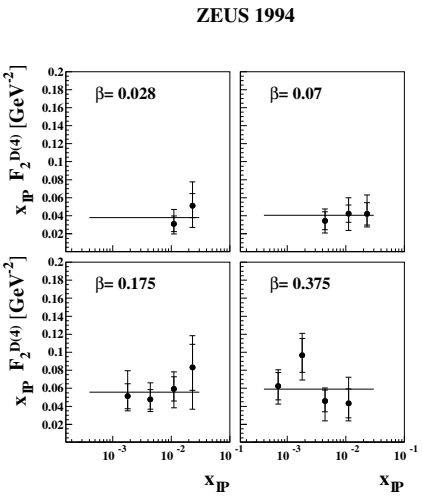

Figure 7: Preliminary ZEUS results on the structure function $F_2^{D(4)}$.

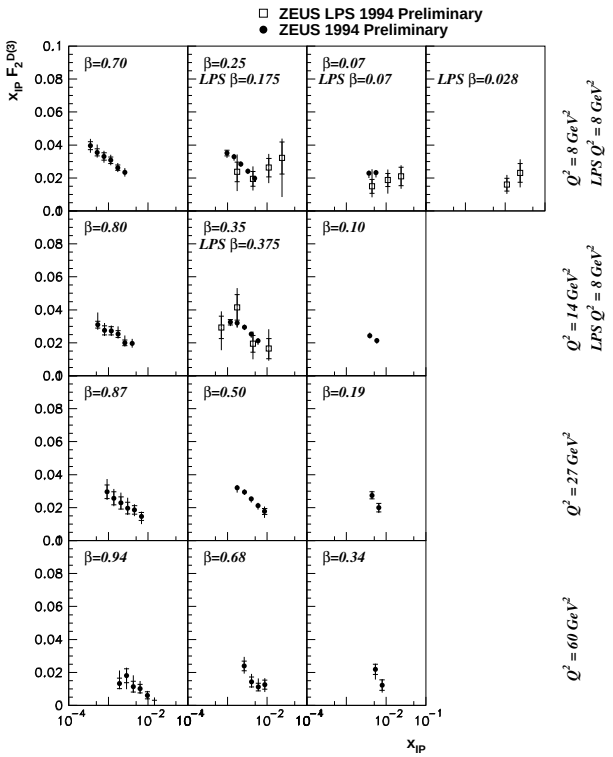

Figure 8: Preliminary ZEUS results on the structure function $F_2^{D(3)}$ obtained with the M_X method (black dots) and with the LPS tag (open squares).

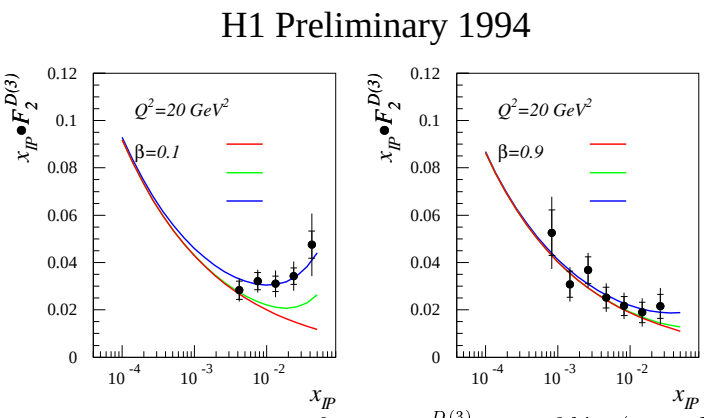

Figure 9: Preliminary H1 results on the structure function $F_2^{D(3)}$ in two β bins (0.1 and 0.9) at $Q^2 = 20$ GeV^2. The data (black dots) are fitted with the sum (upper line) of a pomeron contribution (lower line) and a reggeon contribution with interference (middle line).

This dependence of the $x_{I\!P}$ slope on the kinematic range was first observed by the H1 Collaboration in their preliminary 1994 data [19], where the structure function $F_2^{D(3)}$ was measured with a fine binning in a wide kinematic range ($2.5 < Q^2 < 65$ GeV^2,$0.01 < \beta < 0.9$, $0.0001 < x_{I\!P} < 0.05$). The $x_{I\!P}$ dependence was found to change with β, as illustrated in two bins in fig. 9. One of the possible explanations is factorization breaking effects, predicted by some pQCD models (see e.g. [20]). The other possibility is the contribution of additional reggeon exchanges at high values of $x_{I\!P}$: as the reggeon has an intercept $\alpha_{I\!R}(0) \simeq 0.5$, its effect is to lower the effective exponent a in the $1/x_{I\!P}$ dependence in equation (11). H1 has made a fit to all bins, parametrizing $F_2^{D(3)}$ as a sum of a pomeron and a reggeon contribution:

$$F_2^{D(3)} = F_2^{I\!P}(\beta, Q^2) \cdot 1/{x_{I\!P}}^{(2\alpha_{I\!P}-1)} + C_{I\!R} F_2^{I\!R}(\beta, Q^2) \cdot 1/{x_{I\!P}}^{(2\alpha_{I\!R}-1)}, \qquad (12)$$

where for the reggeon the pion structure function as parametrized in [21] has been used. An example of fit, where the f interference is included, is shown in fig. 9. The data are described, in all β and Q^2 bins, by a pomeron intercept $\alpha_{I\!P}(0) = 1.18 \pm 0.02(stat) \pm 0.04(syst.)$ and a meson intercept $\alpha_{I\!R}(0) = 0.6 \pm 0.1 \pm 0.3$. The introduction of these additional subleading trajectories restores factorization.

The ZEUS Collaboration has instead fit the data obtained with the M_X method at low values of $x_{I\!P}$ ($x_{I\!P} \lesssim 0.01$), where reggeon exchange contributions are expected to be small, in two M_X bins and for the four different Q^2 values (see fig. 8). The result on $\alpha_{I\!P}(0)$ is shown in fig. 10, where the dots indicate the ZEUS results, while the dashed line indicates the H1 result. The two experiments agree; the ZEUS data may indicate a variation of the intercept with Q^2, however the errors are still large to draw any conclusion. The values are above the soft pomeron intercept, which is indicated in the figure with a band in the range $1.07 - 1.11$. A value of $\alpha_{I\!P}(0) \simeq 1.2$ as obtained in these DIS data is higher than the value obtained at $Q^2 \simeq 0$; it also leads to the same steep W dependence ($\simeq W^{0.8}$) as measured in the elastic J/Ψ photoproduction data. These facts suggest that pQCD may play a role when the Q^2 is large.

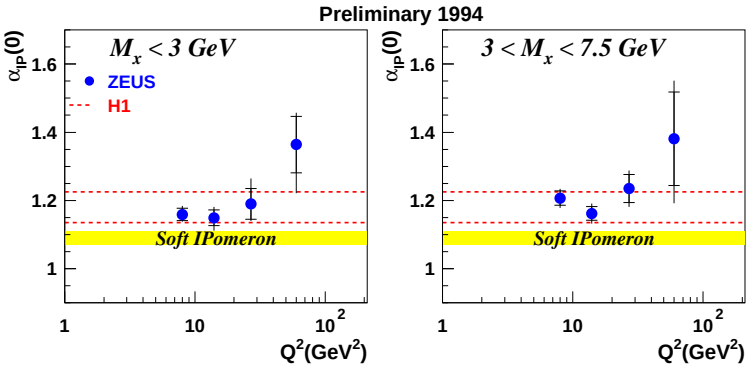

Figure 10: Preliminary H1 and ZEUS results on the pomeron intercept $\alpha_{I\!P}(0)$ in two M_X bins and as a function of Q^2. The dots are the ZEUS data, the dashed line represent the H1 value (with the statistical and systematic errors added in quadrature) obtained from the pomeron plus reggeon fit. The shaded band represents a soft pomeron possible value ranging from 1.07 to 1.11.

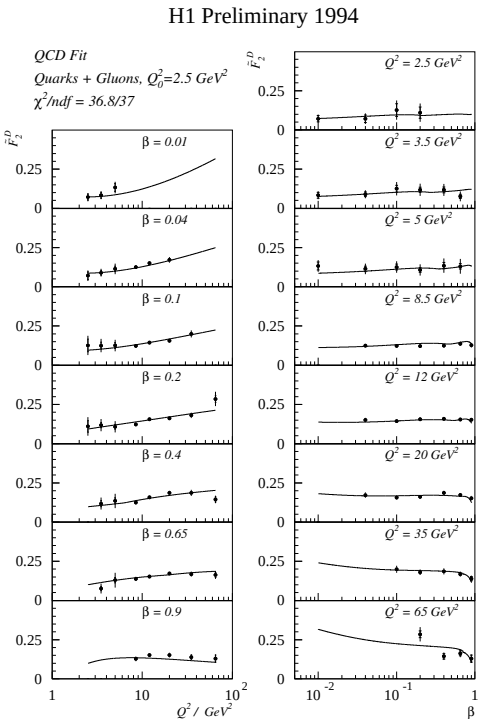

Figure 11: The structure function F_2^D from the H1 1994 preliminary data. The solid line indicates the result of a QCD fit including quarks and gluons.

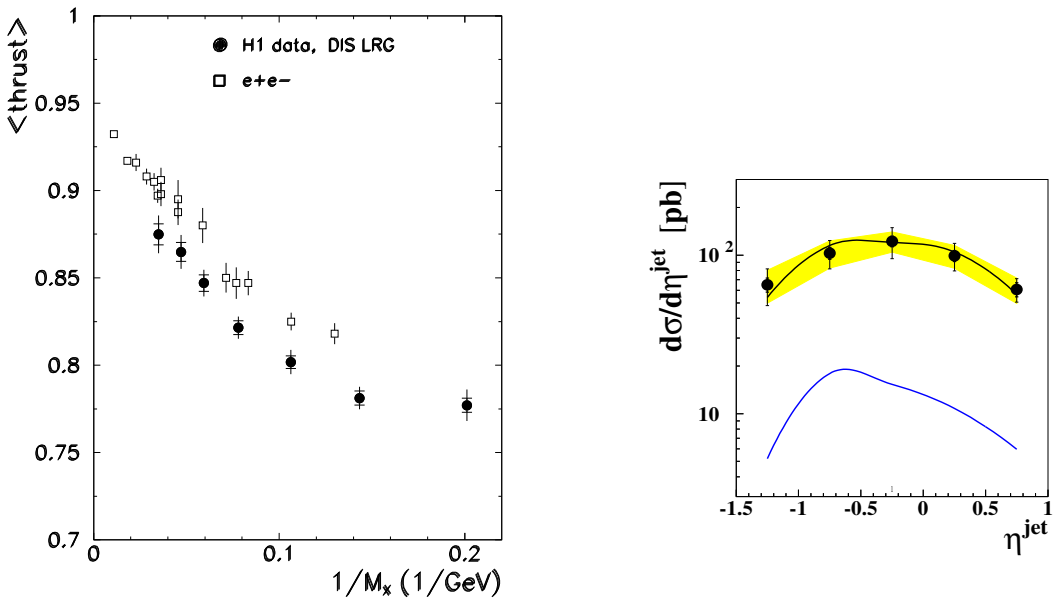

Figure 12: On the left: the mean value of the thrust in the $\gamma^* I\!P$ system as a function of $1/M_X$, obtained from the H1 1994 data (dots), compared to e^+e^- data at similar c.m. energies. On the right: the differential cross section for dijet events in diffractive γp interactions as a function of the jet pseudorapidity, as measured by ZEUS in the preliminary 1994 data. The points are the data, the dashed band is the systematic error due to the calorimeter energy scale, the upper solid line is the prediction for a hard gluon structure function ($\beta(1-\beta)$), the lower solid line is the prediction corresponding to a hard quark structure function ($\beta(1-\beta)+c(1-\beta)^2$) for the pomeron.

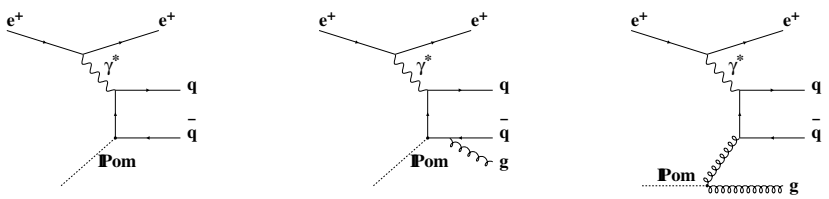

Figure 13: Feynman diagrams for diffractive DIS single dissociation, including the lowest order, and the two first leading order diagrams, QCD Compton and BGF.

H1 has also studied the pomeron structure function as a function of β and Q^2. Integrating $F_2^{D(3)}$ over the measured $x_{I\!P}$ range, they obtained:

$$\tilde{F}_2^D(\beta, Q^2) = \int_{x_{I\!P}=0.0003}^{x_{I\!P}=0.05} F_2^{D(3)}(\beta, Q^2, x_{I\!P}) dx_{I\!P}, \tag{13}$$

where, assuming factorization, the structure function $\tilde{F}_2^D$ is proportional to the pomeron structure function. The latter can be written as a sum over the quark densities in the pomeron, $F_2^{I\!P}(\beta, Q^2) = \beta \sum_q e_q^2 q(\beta, Q^2)$. The result is shown in fig. 11 as a function of β and Q^2, where the black dots represent the H1 data. One observes scaling violations in the Q^2 dependence and a relatively flat dependence versus β. The scaling violations have a positive slope even at very high values of β (the "valence quark" region), as expected if the gluon component dominates. H1 has performed a QCD fit to the data, assuming initial parton densities of the form $q_i, g = A_i x_{i/I\!P}(1-x_{i/I\!P})_i^C$ at a starting value of $Q_0^2 = 2.5$ GeV^2, and evolving them at higher Q^2 with the DGLAP equations. A first fit, assuming that only quark densities contribute to the pomeron structure function, gave a very poor description of the data. A second fit, which includes also the gluon, is shown as the solid line in fig. 11 and describes the data well. The gluon component thus obtained is found to be hard, and it varies from approximately 90% at low Q^2 to 80% at higher Q^2 values. Note that this dominant gluon component is in agreement with models where rapidity gap events at HERA are described in terms of the boson gluon fusion (BGF) process, in which the final state $q\bar{q}$ system evolves in a colour-singlet state, creating a rapidity gap with respect to the proton remnant [22].

3.3 Final states

The measurement of the structure function $F_2^{D(3)}$ gives information on the gluon component in the pomeron through the scaling violations. A complementary information can be obtained by studying specific hadronic final states. The H1 and ZEUS experiments have studied various aspects of the final states, here I will mention only two examples.

The H1 Collaboration has measured the thrust distribution in diffractive DIS events in the $\gamma^* I\!P$ system. The mean value of the thrust is shown as a function of $1/M_X$ in fig. 12. The mean thrust is seen to increase as M_X increases, as expected if the events become more collimated. However, when the H1 values are compared to the mean thrust measured in e^+e^- collisions at similar c.m. energies ($\sqrt{s_{e^+e^-}} \simeq M_X$) [23], the diffractive events seem to be broader, as the mean thrust is always lower. This can be understood by considering the Feynman diagrams in leading order (fig. 13): while for e^+e^- processes only the analogue of the first two diagrams is present, the diffractive single dissociation process contains also the last diagram from the gluon component in the pomeron.

Dijet production in photoproduction is also sensitive to this last diagram and therefore to the gluon content in the pomeron. The ZEUS experiment has measured the differential cross section $d\sigma/d\eta^{\rm jet}$ for dijet events at $Q^2 \lesssim 4$ GeV^2 and $E_T^{\rm jet} > 6$ GeV, as a function of the jet pseudorapidity $\eta^{\rm jet}$. The data are shown in fig. 12, where they are compared to two different pomeron structure function parametrizations: one assumes that the pomeron is

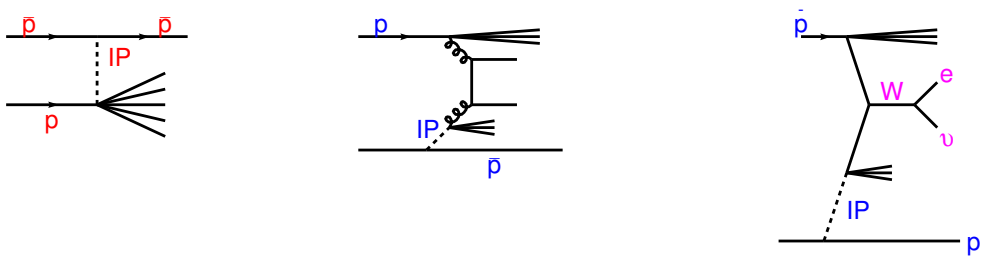

Figure 14: Feynman diagram for single diffractive proton dissociation at Tevatron (left) and in particular for dijet production (middle) and for W production (right).

made of only quarks (lower line), the other assumes that the pomeron has a dominant hard gluon structure function (upper solid line). The hard quark line underestimates the data by almost an order of magnitude, which cannot be explained by the uncertainties in the flux assumed. ZEUS has done also a combined fit to these data and to the published $F_2^{D(3)}$ 1993 results [24], obtaining a gluon component of $\simeq 90\%$ at $Q^2 = 4$ GeV^2.

4 Hard Diffraction at the Tevatron

Hard single diffraction in $p\bar{p}$ collisions at the Tevatron is another process that can be used to investigate the pomeron structure. The process is the pomeron exchange reaction in the t channel, in which the $\bar{p}$ (p) remains intact and escapes down the beampipe, while the p ($\bar{p}$) dissociates into a system separated in rapidity from the rest of the hadronic final state (see fig. 14). The events are then characterized by a rapidity gap on one side.

These kind of events have been observed by both the CDF and D0 Collaborations in their 2-jet with high E_T samples [25,26]. CDF has also observed hard diffraction with production of a W [27]. These two processes give complementary information on the pomeron structure: the dijet sample gives information on the gluon content of the pomeron (middle diagram in fig. 14), while the W production is sensitive to the quark content in the pomeron (right diagram in fig. 14).

CDF and D0 search for single diffractive events by looking at the measured multiplicity distributions. CDF looks, in the region opposite the dijet system, for correlations between the multiplicity measured in the forward part of the calorimeter ($2.4 < |\eta| < 4.2$) and the number of hits measured in a scintillator counter close to the beampipe, the BBC ($3.2 < |\eta| < 5.9$). This correlation is shown for the dijet samples with $E_T^{jet} > 20$ GeV, $3.5 > |\eta_{jet}| > 1.8$ in fig. 15. A clear peak at zero multiplicity in both parts of the CDF detector can be seen and ascribed to single diffractive events. By parametrizing the non-diffractive background using the shape from the higher multiplicity part, the single diffractive signal can be extracted. The ratio $R_{GJJ} = \sigma(Diffractive\ Dijet)/\sigma(Dijet)$ is measured, as in this ratio most of the systematic effects cancel. The ratio was corrected for acceptance using a Monte Carlo based on a factorizable model and with a hard gluon structure function,

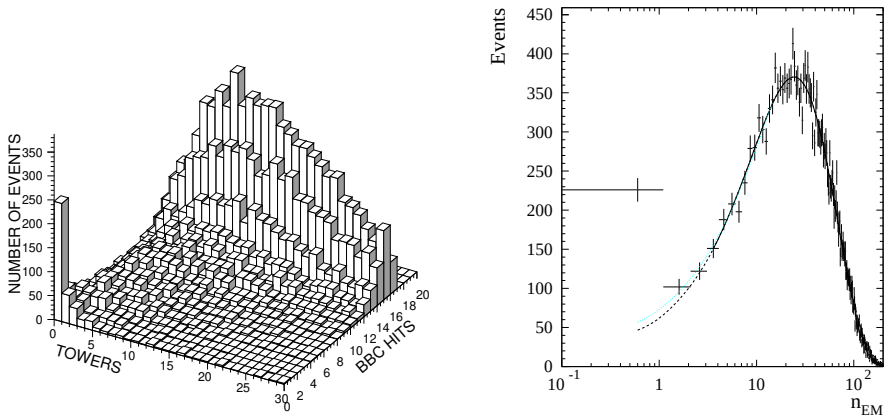

Figure 15: On the left: Correlation between the forward calorimeter tower multiplicity and the number of hits in the BBC counter for the dijet CDF sample. On the right: multiplicity measured in the D0 electromagnetic calorimeter for the dijet sample; the lines represent two types of negative binomial fits to the non-diffractive part.

obtaining

$$R_{GJJ} = [0.75 \pm 0.05(stat) \pm 0.09(syst)]\% \text{ (CDF prel.)}. \tag{14}$$

D0 looked for single diffractive events in the dijet sample at $\sqrt{s} = 1800$ GeV ($E_T^{jet} >$ 12 GeV, $|\eta_{jet}| > 1.6$), studying the multiplicity in the electromagnetic calorimeter region ($2 < |\eta| < 4.1$) opposite the dijet system. A peak at zero multiplicity can be seen in fig. 15, consistent with a diffractive signal. A negative binomial (NB) distribution was fit to the distribution, excluding the very low multiplicity bins, to estimate the non-diffractive background. The uncorrected diffractive signal, obtained from the excess over the NB fit extrapolated to zero multiplicity, is found to be:

$$R_{GJJ} = [0.67 \pm 0.05(stat + syst)]\% \text{ (D0 prel.)}. \tag{15}$$

W production in diffractive events at the Tevatron has been predicted [28] and searched for by the CDF Collaboration. The sample of events currently available is still too small to look for multiplicity distributions. CDF exploits then certain correlations which are present in these events (see fig. 14 right). Suppose that the $\bar{p}$ dissociates, giving a W in the final state and the p remains intact. The events are then characterized by a W in the final state, which is detected in the analysis by the presence of a high p_T electron (or positron) and a missing transverse momentum; furthermore a rapidity gap on the opposite side of the electron or positron is present (this is called angle-gap correlation). In addition, because of the high W mass, the W is likely to be produced by a valence quark in the anti-proton and a valence quark in the pomeron and, as the pomeron is quark-flavour symmetric, approximately two times more electrons than positrons are expected in the final state (this is called charge-gap correlation). Analogous correlations are found in the case in which the anti-proton emits a pomeron. In spite of the small signal (of the order of 20 events), CDF can use

these correlations to determine a ratio of diffractive W production to non-diffractive W production. After correcting this measured ratio by acceptance using a factorizable Monte Carlo model which assumes a hard quark structure function, CDF obtains:

$$R_W = [1.15 \pm 0.51(stat) \pm 0.20(syst)]\%. \tag{16}$$

The two measured ratios can be combined to give the relative quark and gluon content in the pomeron. In this combination, many assumptions on the absolute normalization, like the pomeron flux and the momentum sum in the pomeron, cancel out. The gluon content obtained by CDF is

$$c_g = 0.7 \pm 0.2, \tag{17}$$

in agreement with what is found by the HERA experiments.

CDF and D0 have also observed candidate events for hard double pomeron exchange (DPE). The process is quite interesting as both the proton and the antiproton emit a pomeron, which then interact giving two high E_t jets in the final state. The events are characterized by two jets in the central region of the detector, and two rapidity gaps with respect to the two beam lines. It is therefore a hard pomeron-pomeron scattering process. D0 observes a signal in the multiplicity distributions in the two opposite forward parts of the calorimeter. CDF looks at the proton side for multiplicity (in the same way as described above for single diffraction) while tagging the anti-proton on the other side with the forward proton spectrometer, requiring that $x_L \simeq 1$. Both experiments find a ratio of hard double pomeron exchange events to non diffractive events of the order of 10^{-6}, but more studies are needed to confirm that it is really DPE.

The double pomeron exchange process has been studied in [29], as factorization breaking effects have been predicted especially in hadron-hadron collisions [30]. However the cross section calculated for DPE in this non factorizable model is a couple of order of magnitudes higher than the measured one.

5 A factorization test

We have seen in this report interesting results on single diffraction from HERA and Tevatron and on the partonic structure of the pomeron. One of the main questions is if the pomeron vertex is factorizable, that is if the HERA and Tevatron data can be explained by a universal pomeron, with a universal flux and structure function.

Recently some groups have fit the HERA $F_2^{D(3)}$ data and extracted a pomeron structure function. They have then predicted the ratio R_W at the Tevatron, assuming factorization in hard scattering. The cross section for W production can be written as (see fig. 14 right):

$$\sigma_{diff} = \sum_{a,b} f_{I\!P/p}(x_{I\!P}, \mu) \otimes f_{a/\bar{p}}(x_a, \mu) \otimes f_{b/I\!P}(x_b, \mu) \otimes \tilde{\sigma}_{ab}, \tag{18}$$

where $f_{I\!P/p}(x_{I\!P}, \mu)$ is the flux of pomerons from the proton, $f_{a/\bar{p}}(x_a, \mu)$ is the distribution function of parton a in the anti-proton, $f_{b/I\!P}(x_b, \mu)$ is the distribution function of parton b in the pomeron, while $\tilde{\sigma}_{ab}$ is the cross section for the W production from quarks a and b, which is well known.

The groups use sligthly different assumptions for the flux and the pomeron and proton structure functions and their evolution in Q^2. Alvero et al. [31], when they use a gluon dominated parametrization for the $I\!P$ structure function, obtain a prediction of $R_W = 9.5\%$ for $x_{I\!P} < 0.1$. Kunszt and Stirling[32], using three different models for the HERA data, obtain a value for the ratio R_W varying from 5% to 7% for $x_{I\!P} < 0.1$. Goulianos [33], with simplified assumptions, obtains a value $R_W = 6.7\%$. These values have to be compared with the measured ratio by CDF, $R_W = [1.15 \pm 0.55]\%$: they all seem to overestimate R_W. However there are large uncertainties in the $x_{I\!P}$ range covered by the large rapidity gap at CDF and hence in these predictions which depend on $x_{I\!P}$.

One of the possible explanations for the discrepancy could be that factorization does not hold. Another possibility [34] is that interactions of the spectator quarks in the $p\bar{p}$ collision could destroy the rapidity gap, which has then a survival probability of the order of 10% [b]. The observed R_W ratio may thus be reduced by this survival probability factor.

6 Conclusions

The recent results from HERA, E665 and the Tevatron on diffraction have stimulated a lot of interest in pomeron exchange, as it is the ideal ground to study the interplay between the soft non perturbative regime and the hard perturbative region. Light vector meson or inclusive diffractive photoproduction are well described by soft pomeron phenomenology. However, as soon as an hard scale is involved in the process, for instance the mass of the charm in the J/ψ photoproduction or Q^2 in inclusive photon dissociation, we observe a steep dependence of the cross section with the energy, suggesting that perturbative QCD may play a role.

While pomeron exchange is well described in terms of Regge phenomenology, there is no prediction of its partonic structure, which has therefore to be inferred from the experimental measurements. Results from the diffractive structure function at HERA and from dijet and W production at the Tevatron show that the pomeron is dominantly made of gluons. Using these data, a test of the factorization of the pomeron vertex has been presented.

The pomeron structure function as obtained by fitting the HERA data can be used to make prediction for single diffractive processes at future colliders. According to [36], for example, $5 - 15\%$ of Higgs are produced in single diffractive processes at LHC. Therefore it will be important to look for rapidity gap events also at future colliders.

Acknowledgments

I would like to thank the organizers of the symposium for the invitation to give this talk and for a nice conference. I would like also to thank the many people who helped me in preparing the plots: K. Goulianos and P. Melese (CDF); A. Brandt and T. Taylor (D0); H. Schellman (E665); J. Dainton and P. Newman (H1); H. Beier, G. Briskin, N. Cartiglia, J. Puga, J. Terron and S.M. Wang (ZEUS). Finally special thanks go to M. Arneodo,

[b] This survival rapidity was first introduced in [35] for central rapidity gap events and predicted to be of the order of $5 - 30\%$.

S. Bhadra and R. Nania who have assisted me while preparing the talk and for a critical reading of this manuscript.

References

1. Review of Particle Physics, *Phys. Rev.* D **54**, 192 (1996).
2. A. Donnachie and P.V. Landshoff, *Nucl. Phys.* B **244**, 322 (1984).
3. J.R. Cudell, K. Kang and S.K. Kim, hep-ph/9601336.
4. CDF Collaboration, F. Abe et al., *Phys. Rev.* D **50**, 5550 (1994).
5. see e.g. P.D. Collins in *An Introduction to Regge Theory and High Energy Physics*, ed. Cambridge University Press, Cambridge 1977.
6. WA91 Collaboration, S. Abatzis et al., *Phys. Lett.* B **324**, 509 (1994).
7. K. Goulianos, *Phys. Rep.* **101**, 169 (1983).
8. see e.g. G. Briskin and M. McDermott, in *Future Physics at HERA* and references therein, DESY (1996).
9. G. Ingelman and P. Schlein, *Phys. Lett.* B **152**, 256 (1985).
10. A. Donnachie and P.V. Landshoff, *Phys. Lett.* B **348**, 213 (1995); J.R. Cudell, *Nucl. Phys.* B **336**, 1 (1990).
11. M.G. Ryskin, *Z. Phys.* C **57**, 89 (193); S.J. Brodsky et al., *Phys. Rev.* D **50**, 3134 (1994); J. Nemchik et al., *Phys. Lett.* B **341**, 228 (1994); J.R. Forshaw and M.G. Ryskin, *Z. Phys.* C **68**, 137 (1995); L.L. Frankfurt, W. Koepf and M. Strikman, *Phys. Rev.* D **54**, 3194 (1996); A.D. Martin, M.G. Ryskin and T. Teubner, *Phys. Rev.* D **56**, 3007 (1997).
12. E665 Collaboration, M.R. Adams et al., MPI-PhE 97-03.
13. NMC Collaboration, M. Arneodo et al., *Nucl. Phys.* B **429**, 503 (1994).
14. L.L. Frankfurt, W. Koepf and M. Strikman, hep-ph/9702216.
15. A.H. Mueller, *Phys. Rev.* D **2**, 2963 (1970); D. Field and G. Fox, *Nucl. Phys.* B **80**, 367 (1974).
16. E612 Collaboration, T.J. Chapin et al., *Phys. Rev.* D **31**, 17 (1985).
17. H1 Collaboration, C. Adloff et al., *Z. Phys.* C **74**, 221 (1997) and contributed paper to this conference LP-220.
18. ZEUS Collaboration, J. Breitweg et al., *Z. Phys.* C **75**, 421 (1997).
19. H1 Collaboration, contributed paper to the ICHEP96 Conference in Warsaw, pa02-061, 1996.
20. N.N. Nikolaev and B.G. Zakharov, *Z. Phys.* C **53**, 331 (1992).
21. M. Glück, E. Reya and A. Vogt, *Z. Phys.* C **53**, 651 (1992).
22. W. Buchmüller and A. Hebecker, *Phys. Lett.* B **355**, 573 (1995); A. Edin, G. Ingelman and J. Rathsman, *Phys. Lett.* B **366**, 371 (1996).
23. PLUTO Collaboration, *Z. Phys.* C **12**, 297 (1982).
24. ZEUS Collaboration, M. Derrick et al., *Z. Phys.* C **68**, 569 (1995).
25. CDF Collaboration, F. Abe et al., contributed paper to this conference LP-203.
26. D0 Collaboration, B. Abbott et al., contributed paper to this conference LP-099.
27. CDF Collaboration, F. Abe et al., *Phys. Rev. Lett.* **78**, 2698 (1997) and contributed

paper to this conference LP-202.
28. P. Bruni and G. Ingelman, *Phys. Lett.* B **311**, 317 (1993).
29. A. Berera and J.C. Collins *Nucl. Phys.* B **474**, 183 (1996).
30. J.C. Collins et al., *Phys. Lett.* B **307**, 161 (1993).
31. J. Whitmore et al., to be published in the Proceedings of the DIS97 Workshop, Chicago, April 97.
32. Z. Kunszt and W.J. Stirling, hep-ph/9609245.
33. K. Goulianos, to be published in the Proceedings of the DIS97 Workshop, Chicago, April 1997.
34. D.E. Soper, hep-ph/9707384, to be published in the Proceedings of the DIS97 Workshop, Chicago, April 97.
35. J.D. Bjorken, *Phys. Rev.* D **47**, 101 (1993).
36. M. Heyssler, Z. Kunszt and W.J. Stirling, *Phys. Lett.* B **406**, 95 (1997).